RSC Advances

PAPER

View Article Online
View Journal | View Issue

Cite this: *RSC Adv.*, 2019, **9**, 41066

Microfluidic device performing on flow study of serial cell–cell interactions of two cell populations†

Margaux Duchamp,[a] Thamani Dahoun,[a] Clarisse Vaillier,[a] Marion Arnaud,[b] Sara Bobisse,[b] George Coukos,[b] Alexandre Harari[b] and Philippe Renaud*[a]

Received 14th November 2019
Accepted 5th December 2019

DOI: 10.1039/c9ra09504g

rsc.li/rsc-advances

In this study we present a novel microfluidic hydrodynamic trapping device to probe the cell–cell interaction between all cell samples of two distinct populations. We have exploited an hydrodynamic trapping method using microfluidics to immobilize a batch of cells from the first population at specific locations, then relied on hydrodynamic filtering principles, the flowing cells from the second cell population are placed in contact with the trapped ones, through a roll-over mechanism. The rolling cells interact with the serially trapped cells one after the other. The proposed microfluidic phenomenon was characterized with beads. We have shown the validity of our method by detecting the capacity of olfactory receptors to induce adhesion of cell doublets overexpressing these receptors. We report here the first controlled on-flow single cell resolution cell–cell interaction assay in a microfluidic device for future application in cell–cell interactions-based cell library screenings.

1 Introduction

Cell–cell interactions play a major role in tissue homeostasis[1] and formation.[2] Interactions at the cellular level occur in the embryonic development,[3] tumor progression[4] and metastasis,[4] stem cell maintenance,[5] as well as in the immune system.[6] Our understanding of how cell–cell interactions shape cell behavior relies on our ability to study these dynamic interactions and examine the underlying cellular response. Typical approaches to investigate such interactions at the cellular level involved putting in contact cells in bulk co-cultures[7] with the use of centrifugation[8] (for co-sedimentation steps) or using the flipping assay.[9] These approaches only provide a population-based overview of the cellular response and miss individual variations. Conventional cell–cell interaction methods[10] also include the dual pipette aspiration assay,[11,12] in which two micro pipettes are used to immobilize cells and force them in contact. In this method the interaction force can be probed by modulating the applied pressure exerted on the cell by the pipette end. Another commonly used cell–cell interaction assay is the atomic force microscopy (AFM)-based single-cell force spectroscopy (SCFS).[13] It is an AFM based assay where a cell is adhered on the substrate and another one is placed on the AFM tip. A force is then applied to push the cell on the AFM tip in contact with the one on the substrate. The interaction between the two cells in the AFM is characterized through the deformation of the cantilever. Amongst cell–cell interaction method is the Förster resonance energy transfer (FRET)-based molecular tension sensors[14] assay relies on the transformation of mechanical forces into optical signals. This method uses a FRET-based molecular tension sensor module. Which is introduced in the cytoplasmic domain of E-cadherins, N-cadherin or vinculin to localize the cell–cell contact sites and focal adhesion points by displaying decreased FRET efficiency upon tension on the sensor module. These assays enable a high control of environmental parameters of the interaction, as the contact force (AFM and dual pipette assay), and lead to precise cell–cell interaction study, like measuring the precise tension load on cell membranes (FRET-based tension sensor). However, these methods lack high throughput, as only one cell pair can be studied at a time. Additionally, skilled expertise and tedious manipulation could be required (dual pipette assay). Those methods being time consuming and low throughput there is a need for higher throughput cell–cell interaction tools.

Recently microfabrication technologies have facilitated the development of single cell analysis tools. Amongst these a focus on microscale methods for cell–cell interaction studies has emerged. The developed methods can be classified into two main categories: open systems (based on microwell arrays) and closed systems (microfluidic channel devices with closed channels). Microwell arrays consist in pico- or nanoliter wells loaded with a cell suspension which will slowly sediment in the wells.[15] Microwell arrays are a simple and easy-to-use method for cell doublet formation as the average number of cells per well can be tailored by the microwell dimensions and the cell doublet formation relies on gravity, a passive mechanism. However, this cell doublet

[a]*Laboratory of Microsystems LMIS4, Ecole Polytechnique Fédérale de Lausanne (EPFL), Lausanne, Switzerland. E-mail: philippe.renaud@epfl.ch*

[b]*Department of Oncology, Lausanne University Hospital, Ludwig Institute for Cancer Research, University of Lausanne, Lausanne CH-1066, Switzerland*

† Electronic supplementary information (ESI) available. See DOI: 10.1039/c9ra09504g

formation method doesn't give control over the cell types composing the doublet. Additionally, this method does not allow tuning of the interaction parameters like the contact force or the interaction time between the two cells. On the other hand, closed microfluidic devices enable improved precision over the interaction parameters which allow a more versatile study of cell–cell interactions. Closed microfluidic devices enable a controlled generation of cell–cell interactions[16] thanks to flow control of cells in closed microchannels leading to cell pair formation. Cell doublets can be studied while confined in physical hydrodynamic traps.[17] Cell pairs are placed in contact in static condition by confinement in physical cages. This static condition implies that cells are immobile, hence leading to a long contact time and a high contact force for the interaction. Such traps can also be created with optical,[18] acoustic,[19] or electric[20] forces. Cell doublets are also studied in confined environments like micro-droplets[21] or valved compartments.[22] Most of the methods based on microfluidics rely on static cell–cell interactions where cells are immobile during the interaction. Furthermore, cell doublets are randomly formed with a single cell from the first population placed in contact with a single cell from the second population. In the case of rare cell populations this random cell pairing could be problematic, and thus lead to cell loss. Compared to conventional cell–cell interaction assays microscale devices enable an increased throughput thanks to the parallelization of cell pairs formation.

In this study we developed a microfluidic device capable of multiplexing dynamic cell–cell interactions. The term dynamic implies that at least one cell of the doublet is in movement during the interaction. This device leads to cell–cell interaction multiplexing as it enables to probe serially cell–cell interactions between two cell populations. A sample (size defined by the amount of trap per chips) composed of single cells from the first population is immobilized in traps and placed in contact with rolling cells from the second population. All possible cell–cell interactions between the cell samples of each population is therefore investigated. This novel concept has been tested with the investigation of the role of an olfactory receptor (OR) in the functional wiring of the olfactory system. The device we designed offers the possibility to study the hypothesis that ORs might be involved not only in sensing odorant molecules but also in cell-to-cell recognition for directing axon molecular cues in the olfactory bulb.[23–25] We choose to investigate the mouse olfactory receptor mOR256-17 (Olfr15) because it has been localized in the axons of olfactory sensory neurons (OSN)[25] and it has been shown to be involved in homotypic and heterotypic cells adhesion.[26] However, the mean of action of the receptor still remains unknown and requires new investigation tools to be further characterized. The chip we created allowed us to trap cells expressing the mOR256-17, subsequently make another cell expressing the same receptor roll over the trapped one. To our knowledge, this is the first microfluidic device enabling the study of cell–cell interaction of all cells of samples (sample size defined by the number of hydrodynamic traps in the device) from two distinct populations while on flow.

2 Principle

2.1 Microfluidic chip principle

The presented microfluidic device is composed of a main channel, in which particles flow, in parallel with a low-pressure channel. Those channels are linked by perpendicular narrower channels called trap channel and bypass channels. Particles are trapped at the junction between the main and the trap channels while, bypass channels are designed for partial flow aspiration. This chip can be operated in two modes: trapping and "roll-over" (Fig. 1).

The trapping mode (Fig. 1A) allows particle trapping at trap channels entrances. The specific widening of the trap channel entrance is called the trap cup and is where the trapped particle will be placed. Virtual widths are defined as the flow stream width from the main channel entering either the trap channel (w_0) or the bypass channel (w_1). Virtual width values depend on the ratio of flowrates respectively Q_T/Q_M and Q_B/Q_M, no additional trapping force is applied. When the radius of a flowing particle is smaller than the virtual width (w_0 in Fig. 1A) of the trap, it is diverted towards the trap channel[27] and hydrodynamically trapped[28] thanks to a mechanical constriction as shown in Fig. 1A. When all trap channels are passively filled with particles the roll-over mode can be implemented.

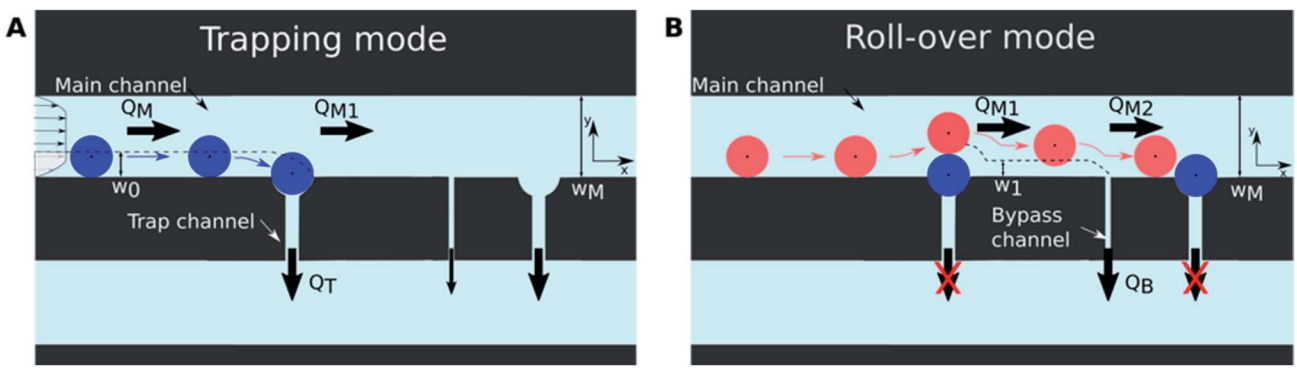

Fig. 1 (A) Schematic view of the particle trapping mechanism. The particle carried by the flow (Q) is trapped in the trap channel. (B) Schematic view of the particle rolling mechanism. Particles carried by the flow roll on the trapped particles thank to the bypass channel. The bypass channels enable a partial flow reaspiration that modify the flow lines along which flowing particles move. This flow line modification enables to position the rolling particle along the channel and enable a stronger interaction with the following trapped particle.

The roll-over mode (Fig. 1B) allows the sequential interaction of flowing particles with all the previously trapped particles. This phenomenon relies on the hydrodynamic filtering[29] principle. In this case, bypass channels are defined in order to have a virtual width (w_1 in Fig. 1B) smaller than the radius of any flowing particles present in the main channel. Such bypass channels have virtual width designed to partially reaspirate the flow in order to re-position rolling particles along the main channel wall. This positioning along the channel wall after each trap enables flowing particle to interact sequentially with all trapped particle and hence enables a multiplexing of the particle–particle interactions.

2.2 Theoretical analysis

We have developed a simplified model of the fluidic behaviour observed in our device. In which we assumed a fully developed flow in all channels and simplified the design by removing the trap cup at the entrance of the trapping channels. We simplified the model by breaking down the full design (Fig. 2A) into a smaller functional unit that will be repeated with each functional unit presenting the same flow and pressure drops. This functional is composed of a single trap and a single bypass channel (Fig. 2B). This model enabled us to define a range of possible channel dimensions for which trapping and roll-over would occur. However final dimensioning of the microfluidic channels was achieved experimentally.

The virtual widths (w_0 and w_1) are key elements in both trapping and rolling modes. In the first case they enable particle trapping, while in the second case, they prevent particles to be trapped in bypass channels and induce the "roll-over" behaviour. The design of trap and bypass channels needs to be tailored to the particle radius in order to adequately perform both trapping and rolling of particles.

The simplified model is based on the following assumptions: (1) steady, pressure-driven and laminar flow, (2) use of a non-compressible Newtonian fluid, (3) homogenous height along the chip ($h = 20$ μm). The virtual width is linked to the ratio of flowrates between the main channel portion prior to the trap or bypass (Q_M or Q_{M1}) and the trap or bypass channels (Q_T and Q_B respectively). In shallow microfluidic channels (*i.e.* $h < w$), which is the case here, the flow velocity profile[30] is not parabolic but can be expressed[31] as:

$$v_x(y,z) = \frac{4h^2\Delta p}{\pi^3\eta L}\sum_{n\ \mathrm{odd}}^{\infty}\frac{1}{n^3}\left[1-\cosh\left(\frac{n\pi y}{h}\right)+\frac{\sinh\left(\frac{n\pi y}{h}\right)}{\tanh\left(\frac{n\pi w_M}{h}\right)}-\frac{\sinh\left(\frac{n\pi y}{h}\right)}{\sinh\left(\frac{n\pi w_M}{h}\right)}\right]\sin\left(\frac{n\pi z}{h}\right) \quad (1)$$

where η is the viscosity of the fluid (9.8×10^{4} Pa s for water), Δp is the pressure difference between channel ends, h, L, w_M are the respective channel dimensions: height, length, width, and y, z are the coordinate axes along the channel width and height with $0 < y < w_M$ and $0 < z < h$. The flowrate for each channel can then be calculated by integrating this velocity flow profile eqn (1) along the height and the width of the channel. In this case Q_T was calculated using the virtual width w_0. In such conditions, the trapping ratio is given by:

$$\frac{Q_T}{Q_M} = \frac{w_0}{w_M}\frac{1+\sum_{n\ \mathrm{odd}}^{\infty}\frac{96h}{n^5\pi^5 w_0}\left(\frac{\cosh\left(\frac{n\pi}{h}(w_M-w_0)\right)-\cosh\left(\frac{n\pi w_0}{h}\right)}{\sinh\left(\frac{n\pi w_M}{h}\right)}-\tanh\left(\frac{n\pi w_M}{2h}\right)\right)}{1-\sum_{n\ \mathrm{odd}}^{\infty}\frac{192h}{n^5\pi^5 w}\tanh\left(\frac{n\pi w_M}{2h}\right)} \quad (2)$$

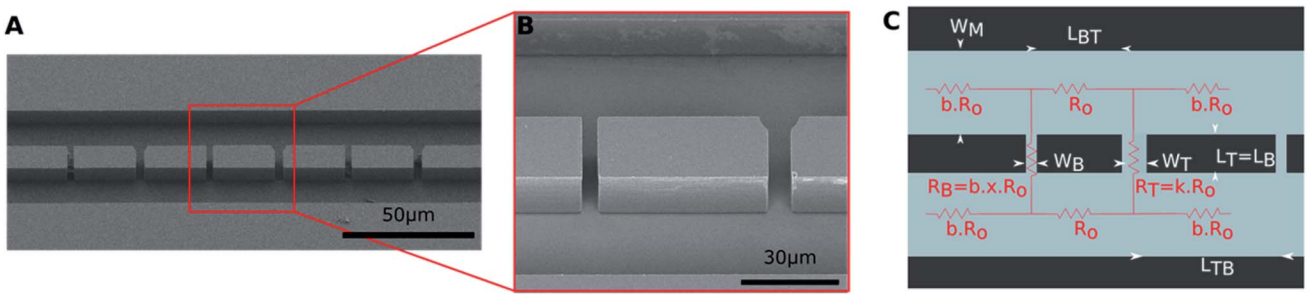

Fig. 2 Microfluidic device fabrication and design. (A) Scanning electron microscope image of the designed silicon on glass microfluidic chip. The microfluidic device is composed of a repetition of a single basic chip unit. (B) Zoom on the functional unit composed of a bypass channel and a trap channel. This functional unit is the basis of the simplified model. (C) Illustration showing the equivalent electrical resistive model of a functional repeating unit of the chip composed of a bypass and a trap channel with the corresponding design dimensions.

The necessary trapping condition is $w_0 > r_P$ (r_P is the particle radius).

In a similar manner the roll-over ratio $\frac{Q_B}{Q_M}$ is obtained from eqn (2) by replacing w_0 by w_1, with the rolling condition $w_1 < r_P$.

In our experimental setup flowrates are controlled using a pressure regulator at the main channel inlet. Using the Hagen–Poiseuille equation, $Q = \frac{\Delta p}{R}$, the critical design dimensions can be calculated knowing the hydraulic resistance of each channel. Using the hydraulic-electric analogy, the fluidic circuit can be represented by an electric circuit[32] (Fig. 2C). In order to simplify the calculation of the resistance of such a circuit we defined a unit resistance R_o corresponding to the equivalent resistance of the main channel portion located between a bypass and a trap channel. All the remaining resistances (trap R_T bypass R_B and main or low-pressure channel portions) are linked to this unit resistance by a constant coefficient (respectively k, $x.b$, and x). An entrance resistance generating the pressure drop between the main channel and the low-pressure channel is present on the device but not detailed here. The equivalent resistance for the trapping area of the chip is:

$$\mathrm{Req}_n = \left(\sum_{i=1}^{2n} R_{\mathrm{kc}i}\right) + \frac{\left(R_{\mathrm{ka}(2n)} + \frac{R_o}{2}\right)\left(R_{\mathrm{kb}(2n)} + \frac{R_o}{2}\right)}{\left(R_{\mathrm{ka}(2n)} + R_{\mathrm{kb}(2n)} + R_o\right)} \quad (3)$$

where n is the number of traps/bypass channels and R_{ka}, R_{kb}, R_{kc} are found using the Kennelly transformation and are defined as follow:

$$\begin{pmatrix} R_{\mathrm{ka}i} \\ R_{\mathrm{kb}i} \\ R_{\mathrm{kc}i} \end{pmatrix} = \begin{pmatrix} \frac{kR_o\left(R_{\mathrm{ka}(i-1)} + R_o\right)}{R_{\mathrm{ka}(i-1)} + R_{\mathrm{kb}(i-1)} + R_o(k+2)} \\ \frac{kR_o\left(R_{\mathrm{kb}(i-1)} + R_o\right)}{R_{\mathrm{ka}(i-1)} + R_{\mathrm{kb}(i-1)} + R_o(k+2)} \\ \frac{\left(R_{\mathrm{ka}(i-1)} + R_o\right)\left(R_{\mathrm{kb}(i-1)} + R_o\right)}{R_{\mathrm{ka}(i-1)} + R_{\mathrm{kb}(i-1)} + R_o(k+2)} \end{pmatrix} \quad \text{for } i \text{ odd}$$

Once R_o is defined all other hydraulic resistances can be calculated, by combining eqn (2) and (3), upon the definition of the desired main channel flowrate. In this study, the device design and operating conditions are based on theoretical analyses and have been improved with experimental data.

3 Experimental

3.1 Device design

The theoretical model relies on the hydraulic resistance R_o, by defining the parameters of this channel portion one can obtain this resistance with the following equation:

$$R_o = \frac{12\eta L}{wh^3} \frac{1}{1 - \sum_{n\ \mathrm{odd}}^{\infty} \frac{192h}{n^5\pi^5 w} \tanh\left(\frac{n\pi w}{2h}\right)}$$

Once R_o is known all the channel design parameters can be defined as all the other channel resistances are functions of R_o.

3.2 Device fabrication

The silicon (Si) on glass microfluidic device (Fig. 2A) was fabricated using DRIE (Dry Reactive Ion Etching) and is composed of a glass bottom with Si channel walls, capped with a polydimethylsiloxane (PDMS) layer used for gas transfer and fluidic connections. This fabrication method was selected as it enables high aspect ratio microchannel fabrication (AR = 10 Fig. 2B) using Si microstructuration. Additionally, it leads to high contrast for brightfield and fluorescent imaging as the microchannels are transparent while the walls are opaque. Furthermore, this material retains a hydrophilic behaviour (compared to conventional PDMS chips used for biological application that have high hydrophobic behaviors[33]) which is highly desirable in the case of narrow microchannels (bypass channels). The generated microfluidic channels can easily be washed and cleaned (acetone, IPA, bleach, sulfuric acid) before being reused. The fabrication process is as follow. A borofloat wafer is anodically bonded[34] (420 °C, 800 V) to the device layer of an unstructured silicon on insulator (SOI) wafer (20 μm : 0.5 μm : 250 μm). The removal of the SOI handle and oxide layers are respectively achieved by grinding (DISCO grinder) and DRIE (AMS 200) of the Si and plasma etching (ASPTS) of the SiO_2. The remaining 20 μm high SOI device layer on the glass is then patterned (photolithography, coating, exposure and development of AZ1512HS 2 μm) and etched using the Bosch process (DRIE) according to the final chip design. The microchips are then diced (DAD dicing machine, 1 mm s^{-1} dicing speed, 0.5 L min^{-1} water flowrate), plasma bonded (oxygen plasma bonding, 350 mTorr, 45 s, 29 W), and individually aligned with a pre-punched (OD = 0.75 mm) PDMS slab (Sylgard Dow Corning, ratio 1 : 10 curing agent : polymer). The PDMS cap is used to ensure proper fluidic connections and enables gas exchange.

3.3 Bead suspension preparation

10 μm polystyrene beads (Spherotech) suspended in deionized water were diluted to a final concentration of 3×10^6 beads per mL in phosphate buffered saline (PBS, GIBCO) with 0.05% Tween 20 (Sigma). The working beads solution was placed in 2 mL glass vials (Chromacol clear 9 mm Screw Thread Glass Vial) and vortexed prior to each use in the microfluidic device.

3.4 Cells transfection

Twenty-four hours before transfection HEK cells (ATCC) growing in DMEM containing 10% fetal bovine serum (FBS) (GIBCO) were seeded on 48 wells (Greiner) at a concentration of 100 000 cells per mL. Cells were then either cotransfected with pA1-OR256-17-EGFP[35] and pRTP1S[35] at a ratio of 50% w/w or transfected with a citrine encoding plasmid expressing a variant of the yellow fluorescent protein (YFP) (Clontech) and used as a negative control using Lipofectamine 2000 (Invitrogen) following the manufacturer's protocol. To avoid any effect of lipofectamine on our experiments, the medium has been

replaced with fresh medium supplemented with 10% FBS 5 h after transfection. The transfection efficiency was of 65.4% and has been assessed using flow cytometry (data not shown).

3.5 Cell suspension preparation

Cells transiently co-expressing A1-OR256-17-EGFP and RTP1S or expressing citrine were detached using trypsin–EDTA (GIBCO) for 2 min at 37 °C, resuspended in DMEM 10% FBS and centrifugated at 180 g for 2 min. The cell pellet was diluted in PBS complemented with 1 mM of EDTA and filtered with a 40 μm cell strainer (Falcon), before being placed in a 300 μL glass vial (Chromacol clear 9 mm Screw Thread Glass Vial). The final cell concentration before injection in the microfluidic device was 1×10^6 cells per mL. Cells were kept on ice before the experiment to prevent receptors internalization.

3.6 Experimental setup and device operation

The beads experiments were performed with a Nikon Eclipse TE 300 inverted microscope, at a 20× objective and with a MQ003MG-CM B&W camera (Ximea). The camera was controlled with the XimeaCop software acquiring at 200 frames per second (FPS). The cell experiments were performed on a LSM510 laser scanning microscope (Zeiss) equipped with 20× dry objective. The cell movies were acquired at a frame rate of 1.27 FPS. Fluigent Flow-EZ pressure controller ranging from 0 mbar to 1000 mbar was used to apply pressure on the glass vials. 100 μm inner diameter polytetrafluoroethylene (PTFE, IDEX 1571) tubing was used to connect the glass vials to the microfluidic chip through a custom-made vial cap. The bead and cell movies were analysed using FIJJ software and manual particle tracking plugins.

The chip was primed with deionized water at high pressure (200 mbar) to remove bubbles. A first set of particles (beads per cells) were loaded in the chip at 70 mbar to be trapped. Once all trapping sites were filled the applied pressure was decreased to 20 mbar for the rolling behaviour of beads and 2 mbar for cell rolling. After each use the PDMS slab was removed from the chip and channels were cleaned with bleach (14%) and sulfuric acid (H_2SO_4 96%, TECHNIC). The cleaned chips were then bonded with PDMS and used again for further experiments.

4 Results

4.1 Microfluidic device dimensions

We designed and fabricated an array of hydrodynamic traps that passively captures beads and HEK cells. Design dimension consisted in 20 μm high microchannels, 10 μm diameter trap cups, with 5 μm long and 4 μm wide trapping channels. Two different chip designs were made for beads and cells applications, where the disposition as well as the dimensions of the traps and bypass channels were modified along the main flow channel. The first one involved in the bead demonstration as well as used for the theoretical model, consists in 10 traps and bypass channels along a straight 30 μm wide main channel (the design can be visualized on Fig. 1–3). Bypass channels are 4.7 μm wide and 12.2 μm long and are placed in the middle (47.5 μm distance to the traps) between each trap channels. The cell experiment design improved after the bead characterization has been modified to account for the cell variability in size and deformability. The latter is composed of a serpentine[36] 30 μm wide main flow channel with a single trap at each turn, for a total number of 50 traps. Bypass channels are placed on either side of the trap channels (Fig. 4C and D) at 25 μm of the trap channel on either sides and are 2 μm wide and 9 μm long. A local widening (5 μm wide and 20 μm long) of the main flow channel has been implemented above each trap to account for

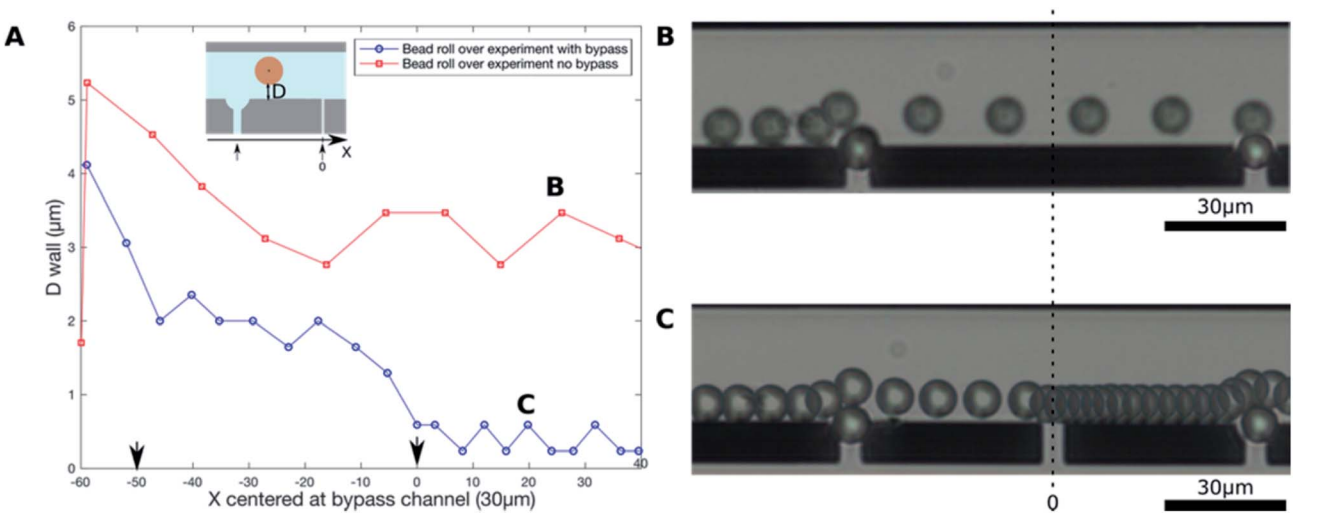

Fig. 3 Bead characterization of the roll-over mechanism. (A) Graph comparing the distance of the bead to the lower side wall as a function of the distance along the channel wall in the presence of the bypass channel and in its absence. The trap is indicated by an arrow at −50 μm, while the bypass channel is indicated with another arrow located at 0 μm on the *X* axis. The points were acquired every 3.7 ms. (B) Brightfield time lapse image of a 10 μm bead rolling on top of trapped 10 μm beads without bypass channels. (C) Brightfield time lapse image of a 10 μm bead rolling on top of trapped 10 μm beads with bypass channels. The dotted line indicates the position of the bypass (C) or the missing bypass channel (B).

cell size heterogeneity and to prevent cell clogging. This design enables a trapping efficiency of 100%.

4.2 Roll over characterization with beads

To study the effect of the bypass channel presence on the rolling bead trajectory and speed, a manual particle tracking plugin available in FIJI was used on movies of 10 μm rolling beads. The presence of bypass channels (Fig. 3C) diverts the rolling bead trajectory towards the microfluidic channel wall. The distance between the rolling bead and the channel wall (named D in Fig. 3A) is in average of 0.5 μm after the bypass channel compared to 2 μm before. This bead movement towards the channel wall is not observed in the absence of bypass channels (Fig. 3B). Indeed, the distance D (Fig. 3A) remains constant between the two traps around 3 μm. This difference between the distance to the wall in both conditions demonstrates the role of the bypass channel to redirect the beads towards the channel wall.

The time lapse images (stacking of images taken every 3.7 ms) of rolling beads (Fig. 3C) enable a visualization of the slowing effect of the bypass channel (from 1704 μm s^{-1} to 1187 μm s^{-1}). The slowing down can be visualized by the shortening of the distance between two sequential bead positions after passing the bypass channel.

The presence of bypass channels in the device enables a dual action to improve the dynamic particle–particle interaction. On the one hand these features divert the rolling beads towards the channel wall. The shift in trajectory enhances the length over which the rolling bead interacts with the surface of the trapped bead. This contact length increases from 8.55 μm when bypass channels are present compared to 4.28 μm when there are no bypass channels. On the other hand, they slow down rolling beads, increasing the bond lifetime with the trapped bead (from 3.7 ms to 14.8 ms).

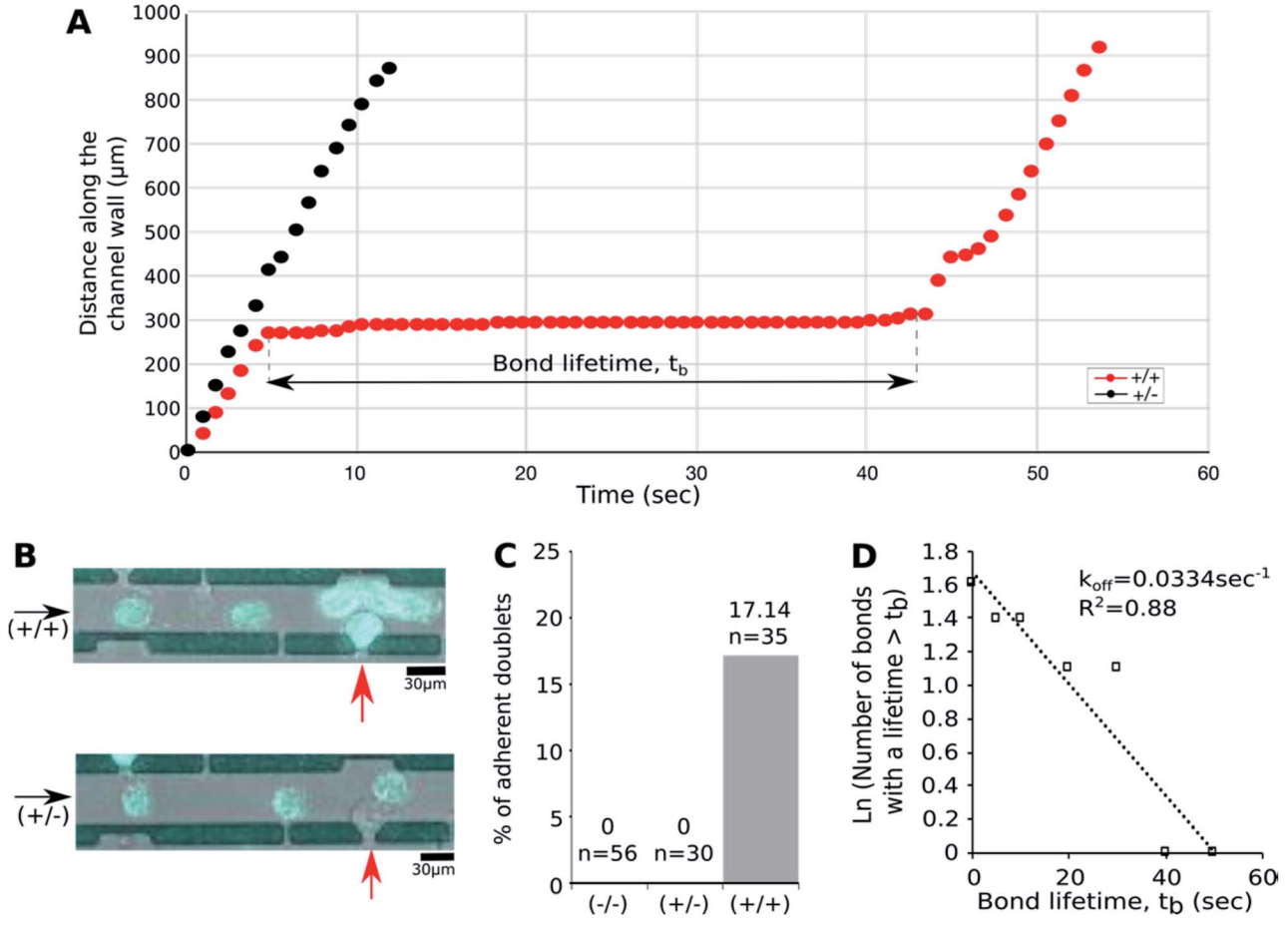

Fig. 4 OR adhesion assay. (A) Graph of the measured instantaneous rolling cell position at each frame as a function time, for the (+/+) and the (+/−) doublet case. (B) Fluorescence and brightfield merge time lapses. Top image is of a rolling OR-GFP expressing cell on an OR-GFP expressing cell (+/+). Bottom image is a time lapse of an expressing OR-GFP cell rolling on a citrine expressing cell (+/−). Trapped cells are indicated with a red arrow. The flow direction is indicated with a black arrow. The images have been acquired every 787 ms. (C) Percentage of adherent doublets of Cit *vs.* Cit (−/−), OR-GFP *vs.* Cit (+/−) or OR-GFP *vs.* OR-GFP (+/+). Significant number of adherent doublets is measured for (+/+) doublets when compared to (−/−) or (+/−) doublets. The number "*n*" of cell doublet has been is the results of multiple experiments. (D) OR–OR bonds were sorted according to their durations. The natural log of the number of events with a lifetime >t_b was plotted against t_b and fitted in a straight line. The negative slope represents the k_{off} dissociation rate indicated on the graph. The goodness-of-fit was indicated by the R^2 values.

4.3 Olfactory receptor homotypic interaction

To investigate cell–cell interactions, we decided to compare the adhesion of cells expressing the olfactory receptor mOR256-17, known to be functionally expressed at the plasma membrane of HEK cells[35] and involved in cell–cell adhesion,[26] to cells expressing a cytosolic fluorescent protein (citrine). We first loaded a population of cells transfected with the mOR256-17 receptor fused to the enhanced green fluorescent protein (EGFP), the EGFP-fluorescent signal allowed us to determine which trapped cells expressed the OR in the microfluidic device. To perform the roll over experiment, we flushed a second cell population expressing either the mOR256-17 receptor (OR-GFP, hereafter indicated with a "+") or the citrine fluorescent protein (Cit, indicated with a "−" sign as it corresponds to the negative control). In this study cell–cell interaction events between two cells over-expressing OR-GFP will be indicated (+/+) and between two cells expressing citrine (−/−). While interactions between OR-GFP expressing cells and citrine expressing cells are labelled (+/−), independently of which cell is rolling. We observed that the instantaneous rolling velocity of a cell expressing OR-GFP is reduced when the cell rolls over a trapped cell expressing also OR-GFP (+/+) while its instantaneous velocity remains high when the cell passes over a trapped cell expressing Cit (+/−) (Fig. 4A and D). The doublets (+/+) showed an average velocity of 0.7 μm s^{-1} at the trap location, while the doublets (+/−) exhibited a velocity of 79.8 μm s^{-1}. Interestingly, cells expressing Cit and rolling over trapped cells expressing also Cit (−/−) display a similar rolling speeds as (+/−) doublets of 79.8 μm s^{-1}. These results indicated that rolling cells expressing OR-GFP interacted specifically only with trapped cells expressing also OR-GFP.

We measured 17% of adherent doublets for (+/+) doublets, while no adherent doublets have been detected with cells doublets involving cells expressing Cit (Fig. 4B). These results are consistent with previous studies[26] on OR homophilic interactions. We measured the time spend by the rolling cell at the trap location, *i.e.* interacting with the cell trapped, and we found that for (+/+) doublets 40% of the rolling cells spend between 30 s and 40 s in contact with the trapped cell. With a maximum bond lifetime of 150 s. Only 20% of the (+/+) doublets stayed less than 10 s in contact with the trapped cells, compared to 100% of the (+/−) and (−/−) doublets (5 s in average). The increased contact time of (+/+) doublets indicates a specific homotypic interaction happening only in the presence of the OR-GFP on both cells (Fig. 4D).

This slowing down of the rolling cell can be associated to the binding kinetics of the OR. The time measured as the bond lifetime (*i.e.* time the cells interact together) corresponds to the time from association to dissociation, also called the bond time t_b in binding kinetics. In the case of a single-step first-order dissociation (assumed here[37]) of single OR–OR bond, the bond lifetime can be linked to the dissociation constant k_{off}. The experiment performed can be assimilated to a thermal fluctuation assay.[38] The following equation[39] enables the calculation of k_{off}:

$$P_b = e^{-k_{off} t_b}$$

With P_b the probability of a bond formed at time 0 to remain intact at time t_b. The plot (Fig. 4C) of the bond lifetime as ln(number of events with a lifetime > t_b) *versus* t_b gives k_{off} as the negative slope of the linear fit. We obtained a value of k_{off} of 33.4 ms^{-1} consistent with the long bond lifetimes observed.

5 Conclusions

We developed a novel dynamic cell–cell interaction device based on a roll-over behaviour. In contrast to conventional approaches that involve dual cell confinement in traps (hydrodynamic, electric, optic, acoustic), this novel microfluidic chip design enables high multiplexing of screening by making a single cell interact with hundreds of others. Furthermore, this device adds the dynamic aspect of cell–cell interaction, thanks to cells flowing over trapped cells. We have investigated the crucial role of the bypass channel featured in this rolling mechanism. The chip we designed allowed us to estimate adhesion properties of the mOR256-17 and determine its binding kinetic constant. Further binding kinetics experiments investigating the effect of shear stress or receptor concentration on the dissociation rate could be performed. The presented experiments and methods can be extended to different cells types. Indeed, the proposed microfluidic chip enables to put in contact cells and study cell–cell interactions at a single cell level through control over the environmental parameters (the force at which cells are placed in contact, the bond lifetime…). The trapping and rolling designs rely on passive fluidic mechanisms and can easily be integrated to other microfluidic components (valves, laser actuators…). Furthermore, this device could be used in other applications like T-cell screening for immunotherapy, where the multiplexing of cell–cell interaction provided by this device could be of high relevance for T-cell library interrogation.[40,41] Optimization of the design dimensions will be required for each application as the roll-over mechanism relies solely on the particle diameter. Furthermore, the mechanical and kinetic[39,42,43] properties of the proteins (cadherins, selectins, TCR, pMHC) involved in the interaction should also be taken into account for the microfluidic chip design. Hence in the case of T cell screening fine tuning of the channel dimensions and fluidic parameters will be required to achieve the necessary contact force and bond lifetime to generate stable immune synapses.[44,45]

Author contributions

Conceptualization: M. D., T. D., C. V., M. A., S. B., A. H., G. C., and P. R.; investigation: M. D., T. D., and C. V.; analysis M. D.; writing: original draft M. D. and T. D.; editing: M. D., T. D., A. H., P. R.; supervision: P. R.

Conflicts of interest

The authors declare no conflicts of interest.

Acknowledgements

This research is kindly supported by the Biltema foundation for the immune engineering project. The authors would like to thank the help and support of EPFL CMi team, Arnaud Bertsch, Ludovic Serex, Jean-Marc Duchamp and Jonathan Cottet.

Notes and references

1 M. A. Garcia, W. J. Nelson and N. Chavez, *Cold Spring Harbor Perspect. Biol.*, 2018, **10**, 1–27.
2 N. J. Abbott, L. Rönnbäck and E. Hansson, *Nat. Rev. Neurosci.*, 2006, **7**, 41–53.
3 F. Hyafil and C. Babinet, *Cell*, 1981, **26**, 447–454.
4 N. Nishida-aoki and T. S. Gujral, *Oncotarget*, 2019, **10**, 785–797.
5 B. Parekkadan, Y. Berdichevsky, D. Irimia, A. Leeder, G. Yarmush, M. Toner, J. B. Levine and M. L. Yarmush, *Neurosci. Lett.*, 2009, **438**, 190–195.
6 M. L. Dustin and F. D. Batista, *Immunol. Rev.*, 2013, **251**, 7–12.
7 P. Moura Rosa, N. Gopalakrishnan, H. Ibrahim, M. Haug and Ø. Halaas, *Lab Chip*, 2016, **16**, 3728–3740.
8 E. Giacomello, J. Neumayer and A. Colombatti, *Biotechniques*, 1999, **26**, 758–766.
9 C. Carmona-fontaine, E. Theveneau, A. Tzekou, M. Tada, M. Woods, K. M. Page, M. Parsons, J. D. Lambris and R. Mayor, *Dev. Cell*, 2011, **21**, 1026–1037.
10 J. Kashef and C. M. Franz, *Dev. Biol.*, 2015, **401**, 165–174.
11 Y. Chu, W. A. Thomas, O. Eder, F. Pincet, E. Perez, J. P. Thiery and S. Dufour, *J. Cell Biol.*, 2004, **167**, 1183–1194.
12 M. Biro and J.-L. Maître, in *Methods in Cell biology*, 2015, vol. 125, pp. 255–267.
13 D. Fichtner, B. Lorenz, S. Engin, C. Deichmann, M. Oelkers, A. Janshoff, A. Menke, D. Wedlich and C. M. Franz, *PLoS One*, 2014, **9**, 1–13.
14 N. Borghi, M. Sorokina, O. G. Shcherbakova, W. I. Weis, B. L. Pruitt and W. J. Nelson, *Proc. Natl. Acad. Sci. U. S. A.*, 2012, **109**, 913–916.
15 N. Varadarajan, B. Julg, Y. J. Yamanaka, H. Chen, A. O. Ogunniyi, E. Mcandrew, L. C. Porter, A. Piechocka-trocha, B. J. Hill, D. C. Douek, F. Pereyra, B. D. Walker and J. C. Love, *J. Clin. Invest.*, 2011, **121**, 4322–4331.
16 R. Li, X. Lv, X. Zhang, O. Saeed and Y. Deng, *Front. Chem. Sci. Eng.*, 2016, **10**, 90–98.
17 B. Dura, M. M. Servos, R. M. Barry, H. L. Ploegh and S. K. Dougan, *Proc. Natl. Acad. Sci. U. S. A.*, 2016, **113**, E3599–E3608.
18 X. Gou, R. Wang, S. S. Y. Lam, J. Hou, A. Y. H. Leung and D. Sun, *Biomed. Eng. Online*, 2015, **14**, 1–15.
19 F. Guo, P. Li, J. B. French, Z. Mao, H. Zhao, S. Li, N. Nama and J. R. Fick, *Proc. Natl. Acad. Sci. U. S. A.*, 2015, **112**, 43–48.
20 M. Abonnenc, M. Borgatti, E. Fabbri, R. Gavioli, C. Fortini, F. Destro, N. Manaresi, G. Medoro, A. Romani, M. Tartagni, P. Giacomini, R. Guerrieri and R. Gambari, *J. Immunol.*, 2013, **191**, 3545–3552.
21 A. I. Segaliny, G. Li, L. Kong, C. Ren, X. Chen, J. K. Wang and D. Baltimore, *Lab Chip*, 2018, **18**, 3733–3749.
22 C. Ma, R. Fan, H. Ahmad, Q. Shi, B. Comin-Anduix, T. Chodon, R. C. Koya, C.-C. Liu, G. A. Kwong, C. G. Radu, A. Ribas and J. R. Heath, *Nat. Med.*, 2013, **17**, 738–743.
23 G. Barnea, S. O'Donnell, F. Mancia, X. Sun, A. Nemes, M. Mandelsohn and R. Axel, *Science*, 2004, **304**, 1468.
24 P. Feinstein and P. Mombaerts, *Cell*, 2004, **117**, 817–831.
25 J. Strotmann, O. Levai, J. Fleischer, K. Schwarzenbacher and H. Breer, *J. Neurosci.*, 2004, **24**, 7754–7761.
26 M. Richard, S. Jamet, C. Fouquet, C. Dubacq and N. Boggetto, *PLoS One*, 2013, **8**, 1–8.
27 M. Yamada and M. Seki, *Anal. Chem.*, 2006, **78**, 1357–1362.
28 V. Narayanamurthy, S. Nagarajan, Y. Firus, F. Samsuri and T. M. Sridhar, *Anal. Methods*, 2017, **9**, 3751–3772.
29 M. Yamada and M. Seki, *Lab Chip*, 2005, **5**, 1233–1239.
30 G.-B. Lee, C.-C. Chang, S.-B. Huang and R.-J. Yang, *J. Micromech. Microeng.*, 2006, **16**, 1024–1032.
31 H. Bruus, *Theoretical microfluidics*, Oxford, 2004.
32 K. Oh, K. Lee, B. Ahn, *et al.*, *Lab Chip*, 2012, **12**, 515–545.
33 J. Zhou, A. V. Ellis and N. H. Voelcker, *Electrophoresis*, 2010, **31**, 2–16.
34 G. V. Kaigala, R. D. Lovchik, U. Drechsler and E. Delamarche, *Langmuir*, 2011, **27**, 5686–5693.
35 T. Dahoun, L. Grasso, H. Vogel and H. Pick, *Biochemistry*, 2011, **50**, 7228–7235.
36 W.-H. Tan and S. Takeuchi, *Proc. Natl. Acad. Sci. U. S. A.*, 2007, **104**, 1146–1151.
37 J. Corzo, *Biochem. Mol. Biol. Educ.*, 2007, **34**, 413–416.
38 J. Hong, S. P. Persaud, S. Horvath, P. M. Allen, B. D. Evavold and C. Zhu, *J. Immunol.*, 2015, **195**, 3557–3564.
39 J. Huang, V. I. Zarnitsyna, B. Liu, L. J. Edwards, N. Jiang, B. D. Evavold and C. Zhu, *Nature*, 2010, **464**, 932–936.
40 K. Garber, *Nat. Publ. Gr.*, 2018, **36**, 215–219.
41 M. A. Stockslager, J. S. Bagnall, V. C. Hecht, K. Hu, E. Aranda-Michel, K. Payer, R. J. Kimmerling and S. R. Manalis, *Biomicrofluidics*, 2017, **11**, 1–9.
42 S. Chen, R. Alon, R. C. Fuhlbrigge and T. A. Springer, *Proc. Natl. Acad. Sci.*, 1997, **94**, 3172–3177.
43 A. Efremov and J. Cao, *Biophys. J.*, 2011, **101**, 1032–1040.
44 S. Pryshchep, V. I. Zarnitsyna, J. Hong, B. D. Evavold and C. Zhu, *J. Immunol.*, 2014, **193**, 68–76.
45 B. Liu, W. Chen, B. D. Evavold and C. Zhu, *Cell*, 2014, **157**, 357–368.